Asphaltenes, subfractions A1 and A2 aggregation and adsorption onto RH-SiO 2 nanoparticles: solvent effect on the aggregate size

Jimmy Castillo, Genesis Gonzalez, Brice Bouyssière, Vicmary Vargas

Asphaltenes, subfractions A1 and A2 aggregation and adsorption onto RH-SiO_2 nanoparticles: solvent effect on the aggregate size

Jimmy Castillo[a*], Genesis Gonzalez[a,b,c], Brice Bouyssiere[a,c*], and Vicmary Vargas[a,b,c]

[a]Facultad de Ciencias, Universidad Central de Venezuela, Caracas 1053, Venezuela; (jimmy.castillo@ciens.ucv.ve)

[b]Universite de Pau et des Pays de l'Adour, E2S UPPA, CNRS, IPREM, Institut des Sciences Analytiques et de Physico-chimie pour l'Environnement et les Matériaux, UMR5254, Hélioparc, 64053 Pau, France ; (genesis.gonzalez@univ-pau.fr; brice.bouyssiere@univ-pau.fr; vicmary.vargas@univ-pau.fr)

[c]Joint Laboratory C2MC: Complex Matrices Molecular Characterization, Total Research & Technology, Gonfreville, BP 27, F-76700 Harfleur, France

***Corresponding author**

Facultad de Ciencias, Universidad Central de Venezuela, Caracas 1053, Venezuela

E-mail: jimmy.castillo@ciens.ucv.ve

Universite de Pau et des Pays de l'Adour, E2S UPPA, CNRS, IPREM, Institut des Sciences Analytiques et de Physico-chimie pour l'Environnement et les Matériaux, UMR5254, Hélioparc, 64053 Pau, France

E-mail: brice.bouyssiere@univ-pau.fr

Abstract

The aggregation and adsorption of asphaltenes in dilute solutions has been extensively studied and is now well established. At low concentrations, asphaltenes are mainly found in the form of aggregates of approximately 3 nm in size. One strategy to simplify the study of these systems has been to fractionate the asphaltenes into subfractions called A1 and A2. The nature of these subfraction aggregates, their behavior with the concentration and their interaction with other aggregates and surfaces remain under debate. This work presents experimental results on the aggregation and adsorption of asphaltenes and their subfractions A1 and A2 onto SiO_2 nanoparticles from rice husks (RH-SiO_2), and the evidence allows us to infer that the aggregates are in equilibrium in solution over a wide range of concentrations. The size distribution for each subfraction does not change with dilution but is sensitive to solvent media. Subfraction A1 has a very similar behavior to asphaltenes, while subfraction A2 tends to form larger aggregates. Larger aggregates more likely adsorb on surfaces than small aggregates. According to the results, the interaction of the aggregates in different solvents can be studied as a phase change phenomenon, where the aggregate can be considered a partially immiscible phase in a solvent. The theoretical principles are described, and a hypothesis is elaborated in these terms.

Keywords: asphaltene aggregation, adsorption, nanoparticle, asphaltene adsorption.

1 Introduction

Asphaltenes comprise a series of molecules with a wide range of molecular weight distributions and heteroatoms, such as nitrogen, oxygen, sulfur, and metals, which modulate their properties. From the operational viewpoint, asphaltenes are defined as the crude oil fraction soluble in light aromatic hydrocarbons (e.g., toluene, benzene) and insoluble in low molecular weight alkanes (e.g., n-pentane, n-hexane, n-heptane). Due to the complexity, their behavior is under study until this date [1].

The behavior of asphaltene aggregates and their association is under debate, and the existence of molecular units of natural asphaltenes has not been verified. Consequently, the aggregates have shown stability in solvents, such as toluene, and the original petroleum mixture. The size of the heterogeneous population of aggregates has been measured with a range of analytical techniques, and the mean aggregate size is 2-20 nm [2]. Evidence suggests a range of sizes in a polydisperse distribution [3]. Other hypotheses propose the existence of supramolecular assembly of molecules; according to the authors, this hypothesis presents a better context to understand, model, and predict the asphaltene behavior. The driving forces for this supramolecular assembly proposed by Gray et al. [4] include a different type of interaction between polar and aromatic groups.

In this context, it is now widely accepted that asphaltenes form aggregates even in very dilute solutions of good solvents such as toluene or THF, but experimental data that describe the nature of the aggregates and aggregation process remain open to interpretation and are the subject of various disagreements. According to the literature, asphaltenes begin to form nanoscale aggregated structures at concentrations below 100 mg L^{-1} [5]. These nanoaggregates are considered to have a limited size because of steric inhibitions introduced by the alkyl chains

attached to asphaltene aromatic cores. In a colloidal approach to the problem, a critical nanoaggregate concentration (CNAC) has been defined as the concentration at which the growth of nanoaggregates starts [6]; at higher concentrations (2–10 g L^{-1}), these nanoaggregates undergo additional association to form clusters or micelles. These aggregates and clusters have often been referred to and considered nanocolloidal and colloidal structures, respectively.

In a solid–liquid phase approach, asphaltene solutions can undergo liquid–solid phase separation to give a solvent-rich phase in equilibrium with asphaltene-rich droplets (clusters). The asphaltene-rich particles formed upon phase separation can act as colloids, but thermodynamically, it is a liquid or glass that exhibits coarsening and coalescence instead of colloidal aggregation at elevated temperature or upon dilution. In discussing asphaltene aggregation, it is important to clearly define the type of aggregates under consideration. In some studies, particles in the size range of 5–10 nm are referred to as both aggregates and nanoaggregates, which of course they are. However, in scattering work, there is a clear distinction between an initial, limited association to form nanoaggregates approximately 2–3 nm in size and subsequent aggregation of these particles to form mass fractal clusters in the size range of 5-10 nm [7].

As reported in previous works [8–11], asphaltenes can be fractionated into two main subfractions A1 and A2 using the p–nitrophenol (PNP) method, where A1 has very low solubility (in toluene, under laboratory conditions) (approximately 90 mg L^{-1}), and A2 has similar solubility to that observed for asphaltenes (5-12%, depending on the sample). This method has been tested numerous times and with different samples and always affords the two fractions with the main difference in solubility. The solubility parameters of asphaltenes A1 and A2 are consistent: A1 is less soluble than A2 in more than 50 different solvents [12].

Asphaltene adsorption governs many aspects of crude oil recovery and production. Generally, the effects produced are undesirable, since they can lead to consequences such as deposition, wettability modification, and emulsion stabilization; thus, considerable efforts have been directed at understanding the behavior of crude oils and their constituents at interfaces. In general, the results from adsorption studies over the years have been fitted with classical adsorption models. The interpretation of these classical models does not give a real answer to all changes in the system, so new approaches to the problem remain under discussion [13–19] In other researches, the use of nanoparticles (NPs) to reduce the size of asphaltene flocks formed in *n*-heptane:toluene mixtures has been reported [19–21]. Large reductions in the average flock size of up to 50% were observed when NPs were added to an asphaltene-toluene solution. We propose that the removal of substantial amounts of aggregates by NPs disrupts the flocks by increasing their solubility, which results in large-sized reductions. The adsorption of asphaltenes on nanoparticles has been previously studied, and different behaviors have been found.

From a geochemical interpretation, asphaltenes are derived from geomacromolecules and generally have high molecular weights and complex chemical structures. Some conceptual structure models that represent the largest possible set of physicochemical analytical data for geomacromolecules have been used to represent structures of humic matter, kerogen, and asphaltenes. Kerogen, asphaltene, and solid bitumen are important for the geochemical information encoded with them. Their macromolecular structures can adsorb and even occlude other small molecules (e.g., biomarkers) [22]. In their works, Cheng et al. [22] present a different view, since asphaltenes are not formed from molecular systems but appear from the cracking of larger structures.

Combining experimental and theoretical studies, Moncayo-Riascos et al. [23] studied the effect of the solvent on the rheological behavior of asphaltenes dissolved in aromatic solvents such as benzene and the three isomers of xylene. Experimentally, differences in the viscosity of the solutions were obtained, being higher in p-xylene than in benzene. Likewise, a correspondence was observed by molecular dynamics simulations with the size of the aggregates obtained in the solutions being o-xylene > m-xylene > p-xylene ≈ benzene, which corresponds to the dipole moment and the solubility parameter due to the location of the -CH_3 substituent. Jiang et al. [24] studied the aggregation behavior of a model polyaromatic asphaltene compound was evaluated. When heptane was added to a solution of the model in toluene, it increased the aggregation especially due to the possibility of establishing interactions via van der walls. When water was added to the mixture, an increase in aggregation and a different rearrangement was observed, in which the water molecules allowed the construction of a network to connect aggregates (via hydrogen bonding) and consequently the formation of aggregate clusters. In contrast, in the presence of an asphaltene inhibitor, it destroyed some interactions between the model and water, dispersing the conglomerates in solution. Xiong et al. [25] studied the adsorption on protonated silica using molecular dynamics of a polyaromatic compound with fused rings similar to those reported for asphaltenes. They found that in heptane aggregates are found in the form of a long strip and these tend to adsorb rapidly on the surface. While in toluene the aggregates are more compact and tend to desorb from the silica surface remaining in the solvent phase.

In the present work, experiments of asphaltene aggregation and adsorption onto SiO_2 NPs are presented, and the results show that asphaltene solutions are composed of aggregates of different molecular weights in equilibrium with the solvent. The solvent properties produce a

change in size distribution proportion in the solution. The tendency of asphaltenes to adsorb on surfaces is greater for large aggregates than for small aggregates. These results can be interpreted based on the existence of a solid–liquid equilibrium, which is consistent with the recent proposal of phase separation suppression, where crude oil or certain solvents act by stabilizing different asphaltene aggregates and preventing the phase separation. The stabilization of this solid phase depends on the quality of the environment and the type of asphaltenes.

2 Experimental Section

2.1 Materials and Methods

Reagents: toluene (99.8%, Scharlau), *n*-heptane (HPLC grade, 99% Scharlau), chloroform (synthesis grade, stabilized with ethanol, 99% Scharlau), cumene (99% Alfa Aesar), tetrahydrofuran [THF, GPC grade, ACS, stabilized with 250 mg L-1 of 2,6-di-*tert*-butyl 4-methylphenol (BHT), 99%, Scharlau], sodium hydroxide (NaOH, synthesis grade, 98%, Scharlau) and *p*-nitrophenol (PNP, synthesis grade, 99%, Scharlau).

2.1.1 Asphaltenes Separation

Asphaltenes were separated from Hamaca and Cerro Negro (also known as Carabobo) Venezuelan crude oils, and their characteristics are shown in Table 1. The procedure for asphaltene separation is based on the ASTM D6560-17 standard and has been widely reported in different publications related to asphaltenes [9–12]. N-heptane was added at a crude:heptane volume ratio of 1:40 to induce the precipitation of asphaltenes. After a resting time of 48-72 h and filtration by suction in two stages, Soxhlet extraction with n-heptane was performed for 6-8 days to remove the coprecipitated material. At this stage, the asphaltenes are separated from the maltenes (saturated, aromatics, and resins).

Table 1. Crude oil characteristics and yields of the asphaltene separation and fractionation.

Crude oil	°API	Stability	% Asphaltenes	% A1	% A2	% TC
Hamaca	9.0	Stable	13.7	38	58	3
Cerro Negro	8.5	Stable	8.0	20	72	6

157

158 *2.1.2 Asphaltenes Fractionation*

159 Based on the fractionation by complex formation with PNP proposed for the first time by
160 Gutiérrez et al. [26], subfractions A1 and A2 and the trapped compounds (TC) were obtained.
161 The asphaltenes were dissolved in cumene saturated with PNP and refluxed for 6 h. During the
162 8-day resting time at room temperature, subfraction A1 precipitates as an insoluble asphaltene-
163 PNP complex, while in solution, subfractions A2 and TC remain in solution. After the filtration
164 steps, reduced pressure distillation of the cumene, and successive washing with *n*-heptane, the
165 solid subfractions were obtained. The PNP was removed by successive washing with a 5%
166 aqueous NaOH solution until colorless washing was obtained. The yields of subfractions A1 and
167 A2 and TC (saved for further analysis) are shown in Table 1. The A1 and A2 subfractions have
168 the same average composition and characteristic of previously reported [26] where the most
169 important difference between these fractions is in the H/C ratio with 0.90 for A1 and 0.99 for A2
170 and the Double Bond Equivalent (DBE) of 56 for A1 and 52 for A2.

171 *2.1.3 Asphaltene Solution Preparation*

172 Solutions of the whole asphaltenes and their subfractions A1 and A2 were prepared in THF and
173 $CHCl_3$ at a fixed concentration of 1000 mg L^{-1} and in the concentration range of 50-2000 mg L^{-1}.
174 All solutions were analyzed by GPC-ICP HR MS, where ^{51}V, ^{32}S, and ^{58}Ni isotopes were
175 monitored.

176 *2.1.4 SiO_2 nanoparticle preparation*

177 SiO_2 nanoparticles from rice husks (RH-SiO_2 NPs) were prepared using a modification of a
178 reported process [16]. In the first step, rice husks were leached with 100 mg/L HCl, washed to
179 neutral pH, and heated at 120 °C to remove water. Then, with a heating ramp of 500 °C h^{-1}, the
180 rice husks were heated at 500 °C for 1 h to burn carbonaceous residue and at 700 °C for 9 h to
181 produce loosely interconnected amorphous SiO_2. The amorphous silica size was reduced by a
182 ball milling process for at least 24 h, and mesoporous nanoparticles were obtained with an
183 average size of 40-60 nm, a porosity of 78%, and a specific surface of 234 m^2 g^{-1}. The BET and
184 porosity plots are shown in Figs. S5 and S6, respectively, in the supporting information.

185 *2.1.5 Asphaltenes Adsorption Experiment*

186 The adsorption experiments were based on previous works of Castillo *et al.* [16,18] and Acevedo
187 et al. [27]. In the first batch of experiments, the quantity of NPs was varied. For this purpose, 600
188 mg L^{-1} asphaltene solutions in toluene and $CHCl_3$ were prepared and placed in contact for 72 h
189 with RH-SiO_2 NPs in the concentration range of 0-5 and 0-300 mg/L, respectively. The
190 remaining solutions after adsorption were analyzed by GPC-ICP HR MS and UV–Visible
191 spectroscopy.

192 Subsequently, the adsorption behavior of the asphaltenes was analyzed concerning their
193 A1 and A2 subfractions. Then, 600 mg L^{-1} asphaltenes and their A1 and A2 subfraction solutions
194 in $CHCl_3$ were placed in contact with 300 mg/L RH-SiO_2 NPs for 72 h. After this time, the
195 remaining solution was separated from the solid phase by centrifugation (6000 rpm for 5 min).
196 From the experiments, the solutions before and after adsorption were analyzed, and the solid
197 material (RH-SiO_2 nanoparticle NPs adsorbed with the asphaltene or subfraction) was extracted
198 with THF to study the desorption of the material. From now on, the solution before adsorption is

called "original", the one after adsorption "remains", and the one from the THF extracts "extract". All solutions were analyzed by GPC-ICP HR MS.

2.1.6 GPC-ICP HR MS Analysis

As reported in previous studies [18,27,28], GPC-ICP HR MS analyses were performed using a Thermo Scientific Element XR sector field ICP HR MS instrument that operates at a resolution of 4000 (medium resolution) to access spectrally interfered isotopes of ^{58}Ni, ^{32}S, and ^{51}V. The spectrometer was equipped with a Fassel-type quartz torch shielded with a grounded Pt electrode and a quartz injector (1.0 mm i.d.). A Pt sampler (1.1-mm orifice diameter) and a Pt skimmer (0.8-mm orifice diameter) were used. An O_2 flow was continuously supplied to the nebulizer Ar gas flow. The introduction system was fitted with a modified DS-5 microflow total consumption nebulizer (CETAC, Omaha, NE) mounted on a laboratory-made, low-volume (8 mL), single-pass-jacketed glass spray chamber of total consumption. The spray chamber was thermostated to 60 °C. The ICP HR MS conditions were controlled and optimized daily using a 1.0 ng g^{-1} multielement tuning solution in THF delivered via a syringe pump at a flow rate of 15 µL min^{-1}.

Chromatographic separations were conducted using a Dionex HPLC 3000 with three Styragel styrene-divinylbenzene gel permeation columns connected in series (7.8 × 300 mm) that works at a flow rate of 0.7 mL min^{-1} in THF. These columns were HR4 (particle size, 5 µm; exclusion limit, 600 000 Da of polystyrene [PS] equivalent), HR2 (particle size, 5 µm; exclusion limit, 20 000 Da) and HR0.5 (particle size, 5 µm; exclusion limit, 1000 Da). A Styragel guard column (4.6 × 30 mm) was included before these three columns to protect them and prolong their lifetimes. The separation achieved by the columns was evaluated using a mixture of PS standards of 1,000,000–162 Da. According to the GPC column configuration, high-molecular-weight compounds elute at shorter times, and low-molecular-weight molecules elute at longer times,

which allowed us to define integration intervals for super-high (SHMW), high (HMW), medium (MMW), and low (LMW) molecular weights of the eluted components, which correspond to ≈1,000,000–67,000 Da; ≈27,000–6,600 Da; ≈1,100 Da and ≈162 Da in equivalent polystyrene, respectively. For the calibration of chromatographic methods by GPC, polymers of known molar mass are used, and the retention time in the column is correlated with the size of the polymer and these values are used as a reference. In the case of asphaltenes the retention times of the aggregates are measured and these are associated with their size, but the size of these aggregates depends on the shape of the aggregates and the solvation, so the real size of the aggregates is smaller than what is determined by GPC, so the graphs give us the relative size.

2.1.7 UV–Vis Analysis

The fractions of each sample were measured in UV–Visible equipment from Mettler Toledo UV7 using a 1 cm cell. The absorbance signal is taken as a function of wavelength in the range of 350-700 nm. For each sample, the absorbance exponentially decays with wavelength showing a maximum at approximately 420 nm, which corresponds to the Soret band of the porphyrins. For each concentration, the absorbance signal at 450 nm is taken, where the dispersive component of the signal is negligible, and only the absorptive component is taken to construct the absorbance vs. concentration plots.

2.2 Methods

In all adsorption experiments, once the solution reached the contact time with the RH-SiO_2 NPs (72 h), aliquots of these solutions were removed and evaporated to dryness, redissolved in the same amount of THF, and analyzed using GPC-ICP HR MS techniques. The aggregate formation of different sizes depends on the chemical potentials of different aggregates present, their interaction potentials, and the functional form of this potential with the size of the

aggregates. The chromatographic profile displays similar characteristics throughout the concentration range, which indicates that the aggregate fractions were in equilibrium. Fig. 1 shows a typical GPC-ICP HR MS chromatogram for the asphaltene solutions following the vanadium signal, and the SHMW, HMW, MMW, and LMW regions are detailed.

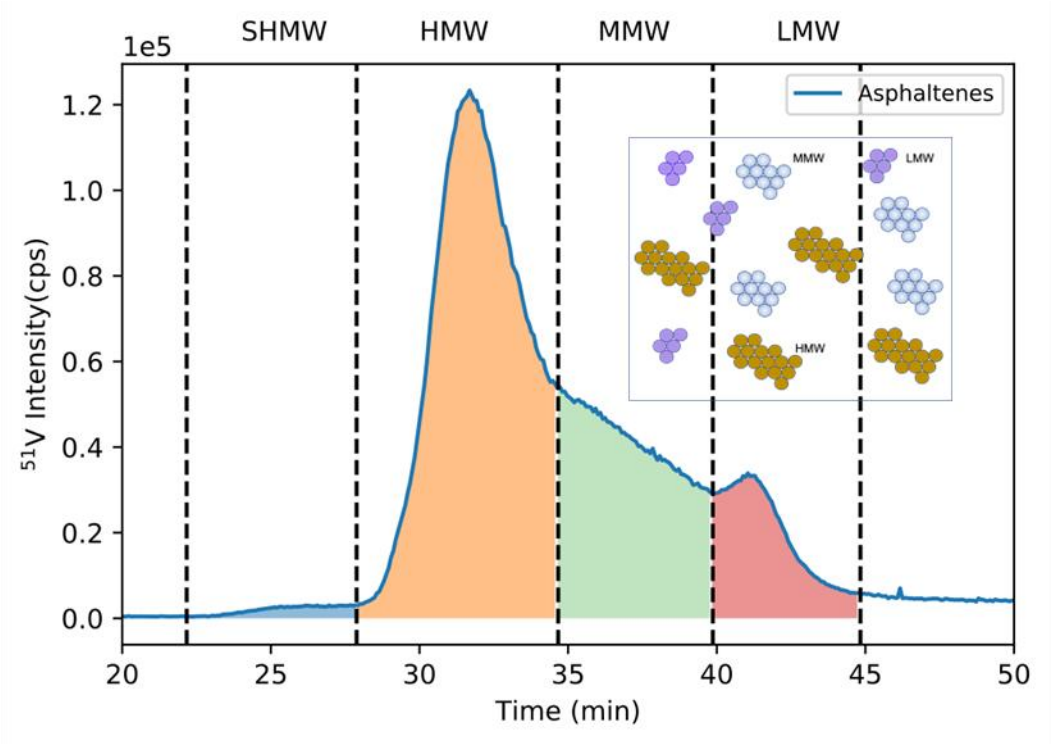

Fig. 1. Asphaltene vanadium GPC-ICP HR MS profile at 1000 mg L^{-1} in THF for Hamaca crude oil, which shows the SHMW, HMW, MMW, and LMW regions, in the inset. Sketch of the HMW, MMW and LMW aggregate models in THF solution

In Fig. 1, three different distributions of aggregates are presented in equilibrium in the solution (assuming that the SHMW region is negligible for asphaltene samples). This equilibrium is sketched in the inset of Fig. 1, where each group of aggregates has equal chemical potential. According to the experimental results, different groups of species are present in the asphaltene fraction, which are represented by three different distributions.

This fact may be expressed as:

$$\mu_{LMW} = \mu^0_{LMW} + k\,T\ln(X_{LMW}) = \mu_{MMW} = \mu^0_{MMW} + k\,T\ln(X_{MMW}) = \mu_{HMW} = \mu^0_{HMW} + k\,T\ln(X_{HMW}) \quad (1)$$

where μ^0_{LMW} is the potential for low-molecular-weight aggregates or monomers, μ^0_{MMW} is the potential for medium-molecular-weight aggregates, and μ^0_{HMW} is the potential for high-molecular-weight aggregates. k is the Boltzmann constant, T is temperature, and X_{HMW}, X_{MMW}, and X_{LMW} correspond to the fraction of each region in THF solution. Assuming that a nanoaggregate of radius r can be represented as a simple spherical structure, number of units N is proportional to the volume ($4/3\pi R^3$), and α is the interaction factor between the particle and the solvent:

$$\mu^0_N = \mu^0 + \frac{\alpha\,k\,T}{N^{\frac{1}{3}}} \quad (2)$$

From Equations 1 and 2, the concentration of aggregates of different sizes in equilibrium in the media can be expressed by:

$$X_{XMW}(r) = e^{-\alpha} = e^{-\frac{4\pi(r-r_0)^2}{k\,T}} \quad (3)$$

where r_0 is the average radius, and r is the radius of different aggregates. For this system of two immiscible components (X_{XMW}), parameter α corresponds to the free energy of transferring a solute molecule from the solute into the solvent phase. γ is the interfacial free energy per unit exposed area of the nanoaggregate, and r is the radius of the aggregate. For a set of nanoaggregates of different sizes $r_i > r_{i_0}$, the fraction X_{XMW} is the sum of the set of aggregates in that fraction that behave in an approximately similar manner.

$$\boldsymbol{X_{XMW} = \sum_i e^{-\alpha_i} = \sum_i e^{-\frac{4\pi r^2 \gamma}{k\,T}}} \quad (4)$$

The properties of the solvent play a very important role in the dissolution and stabilization of the aggregates and affect the aggregation process. The solvent interaction with the aggregates drives the formation of aggregates and their structural conformation, since depending on the properties of the solvent in which it is found, the aggregates may form structures with different geometrical forms. In the experiment, it is assumed that the aggregates behave as nanoparticles with defined sizes immersed in the solvent; despite being soluble in the medium, due to their interactions, the surface energy of the aggregates exceeds the dissolution energy.

3 Results and Discussion

3.1 GPC-ICP HR MS of asphaltenes, A1 and A2 subfractions in different solvents

Fig. 2 shows the vanadium GPC-ICP HR MS profiles that correspond to the hydrodynamic volume separation of asphaltenes and its subfractions A1 and A2 from Cerro Negro crude oil. The samples showed a typical trimodal profile for the asphaltenes and small variations in the profile for the subfractions. Subfraction A1 presents a similar size distribution to asphaltenes with a shift toward high-molecular-weight compounds or larger hydrodynamic volume and a decrease in the low-molecular-weight section. The A2 subfraction shows a notorious shift toward high-molecular-weight compounds or larger hydrodynamic volumes and an evident decrease in the low-molecular-weight section. Similar profiles have been presented in previous works for different asphaltene samples [3,18]. The profiles obtained by GPC-ICPMS are similar in most of the crude oils studied, in the present case, for the Hamaca crude oil, a greater definition of the areas is observed and an area of super high molecular weight appears in a very important way, corresponding to super-aggregates. All samples show that the A2 subfraction tends to form compounds with larger hydrodynamic volumes than asphaltenes.

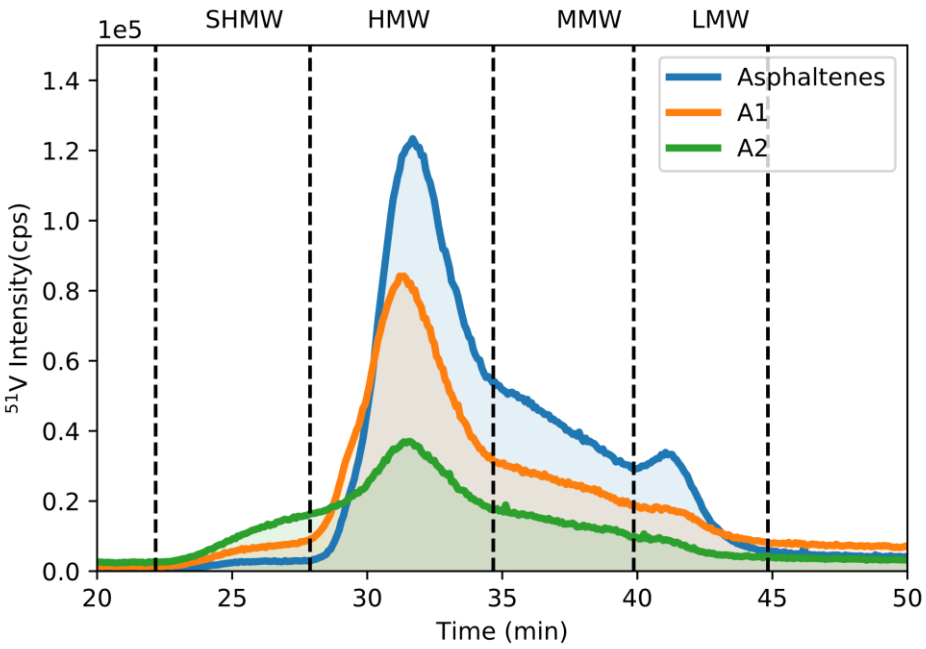

Fig. 2. Vanadium GPC-ICP HR MS profiles of asphaltenes, subfractions A1 and A2 at 1000 mg L^{-1} in THF for Hamaca crude oil.

The A1 subfraction behaves similarly to the asphaltenes, which reinforces the previous results [28], where the stabilization of the asphaltene aggregates is due the interaction of subfractions A1 and A2. Variations in the profiles show that the aggregation of different fractions can be modulated by geometrical parameters, the structure of the formed aggregates, and their fractal dimension [29–31].

Fig. 3 shows the GPC-ICP HR MS profiles for asphaltene and subfractions A1 and A2 in chloroform from Cerro Negro (A) and Hamaca (B) crude oils. The plots show the signals for vanadium, in the case of nickel, and sulfur isotopes the behavior is similar. Chloroform is an aprotic solvent with higher polarity than toluene and lower polarity than THF and a small molecular size, which allows it to more easily diffuse into the aggregate. Fig. 3B show the results for Hamaca, where subfractions A1 and A2 show a tendency to form larger aggregates with a higher hydrodynamic volume than when they are mixed to form asphaltenes. This effect is much

more marked for the solutions in $CHCl_3$ than in THF. In the case of the Cerro Negro crude oil (Fig. 4A-C), the differences are less noticeable, although the changes are still observed. These changes are due to the difference in solubility of the asphaltenes in both solvents and the solubility of the vanadyl compounds trapped in the asphaltene aggregate structure [32–34].

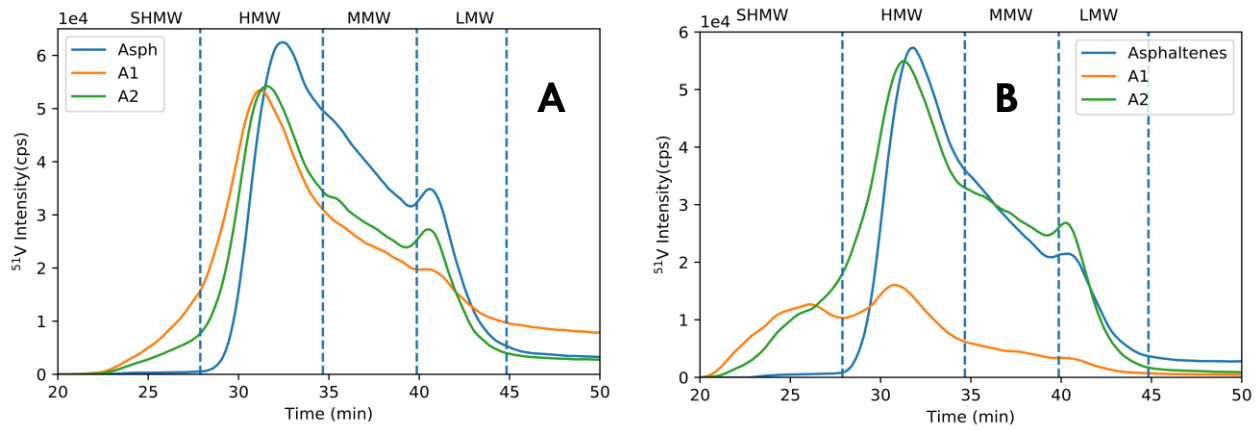

Fig. 3. GPC-ICP HR MS profiles of vanadium, for Hamaca (A) and Cerro Negro (B) asphaltenes and subfractions A1 and A2 in $CHCl_3$ at 1000 mg L^{-1}.

Fig. 4 shows the comparison of vanadium profiles for asphaltenes and its subfractions A1 and A2 for Hamaca and Cerro Negro crude oils dissolved in THF and $CHCl_3$ at the same concentration. This figure clearly shows the differences and the effect of the solvent on the size distribution of the aggregates. There are variations in the vanadium signal in the A1 and A2 subfractions, probably because when the trapped vanadium is being liberated [11,36], the asphaltene aggregates are redistributed, and this effect is more remarkable when a more polar solvent chloroform is used. In the case of Cerro Negro, the differences are less noticeable, although they persist, and the decrease in intensity for the subfractions is also present. The changes using $CHCl_3$ as the solvent are more noticeable than those using THF, and a tailing effect appears.

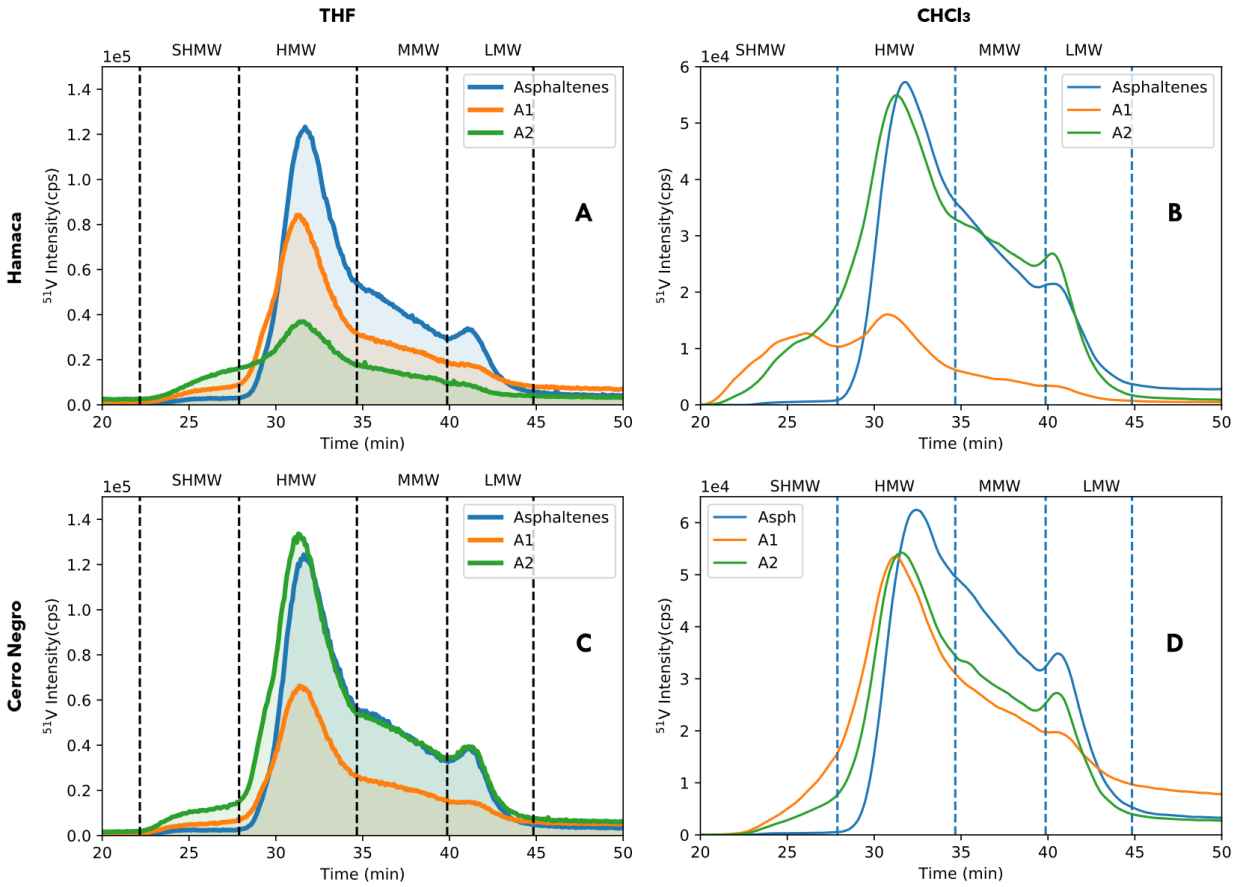

Fig. 4. Vanadium GPC-ICP HR MS profiles for asphaltenes and their subfractions A1 and A2 dissolved in two solvents (THF and $CHCl_3$) at 1000 mg L^{-1} for Hamaca and Cerro Negro crude oils. Sulfur and nickel profiles are shown in Figs. S1 and S2, respectively, in the supporting information. Plots A and C were taken with permission from reference [28].

3.2 Concentration Effects on the GPC-ICP HR MS Profiles

Fig. 5 shows the change in vanadium chromatogram as a function of the concentration for Cerro Negro asphaltenes in THF (**A**) and $CHCl_3$ (**B**) solutions the behavior its similar for A1 and A2. In both cases, there is a linear decrease in the total area as a function of concentration, and the observed molecular mass distribution profile remains constant. This result shows that there are three distributions at equilibrium: HMW = MMW = LMW, and the dilution in the solvent only decreases the concentrations in all distributions without changing their proportions. This

behavior was previously observed by González et al. [28], who found that the behavior of asphaltene solutions and their subfractions in THF as a function of concentration does not follow the tendency of a micellar system; the behavior is similar to a dispersion of particles of different size distributions in a similar process to phase separation [12]. The most remarkable result is that in both solvents, the behavior is identical, and the redissolution of a determinate sample in THF for an injection in the GPC-ICP HR MS does not alter the aggregate characteristics.

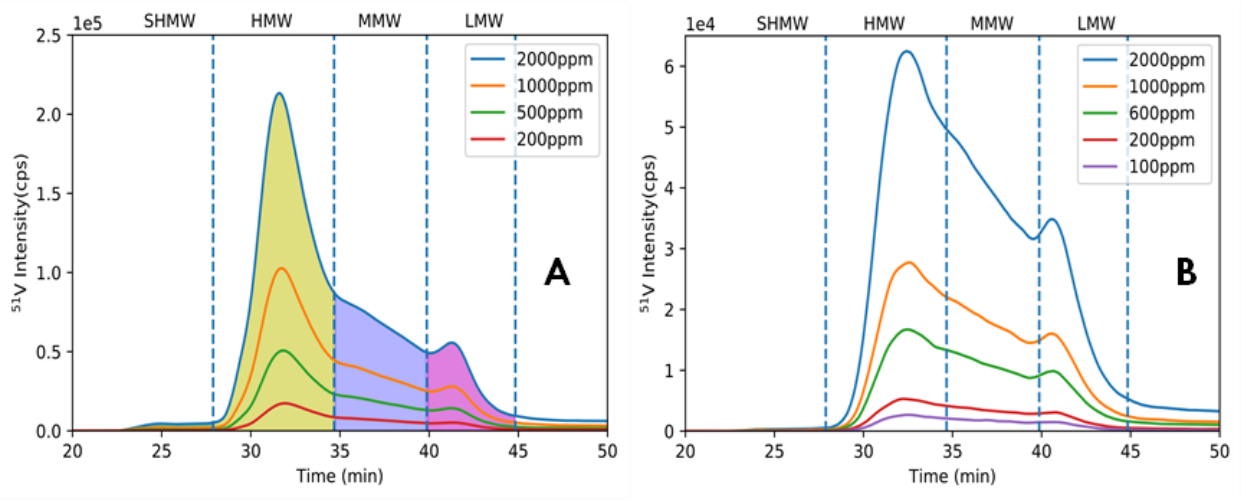

Fig. 5. Vanadium GPC-ICP HR MS profiles for Cerro Negro asphaltenes in THF (A) and in $CHCl_3$ (B) by varying the concentration (50–2000 mg L^{-1}).

3.3 Free surface energy of the aggregates

The fraction of asphaltene molecules is composed of multiple molecules of different molecular weights and composition, an approximation to understand their behavior and their interaction with nanoparticles can be made assuming an aggregate with average size and a size distribution of it[30]. The adsorption experiments could not be interpreted from a classical thermodynamic point of view so we introduce a first approximation based on the calculation of the surface energy[47-51] for the interaction of the species, the surface energy of nanoparticles, and

aggregate is the most important parameter because it provides information about the number of active sites on the surface of the nanoparticle and the type of preferential interaction between nanoparticle and aggregates. The free energy of the aggregate surface can be calculated from the fit of each distribution that composes the sample. The intensity of the signal is proportional to the mass fraction of the sample, and based on the experimental results, we propose the existence of three distributions of different aggregates. The fitting of the experimental data was made with 3 Gaussian distributions with the maximum approximately in the mean value of the regions defined as HMW, MMW and LMW. Small variations are observed in the maxima and semi-widths of the curves of the fits with respect to the experimental signal depending on the solvent. This is due to the ability of the medium to solvate and achieve a better definition of the aggregates present. Using Equation 3, the value of α is obtained using approximate radii of 8, 16 and 21 nm taken from the literature [9]. For the asphaltene aggregates using Equation 3, the interfacial tension γ is obtained. Fig. 6 shows the original curves for asphaltenes dissolved in toluene and $CHCl_3$ and their respective fits taking 3 distributions in each case. Table 2 shows the fit values: α is the fitting constant, γ is the surface free energy or the energy needed to transfer one molecule from the aggregate surface to the solution, and r is the radius of the aggregate. As observed in Table 2, the values of α grow with the size of the aggregate and γ, which indicates that a larger aggregate is less likely to dissolve, which increases its stability.

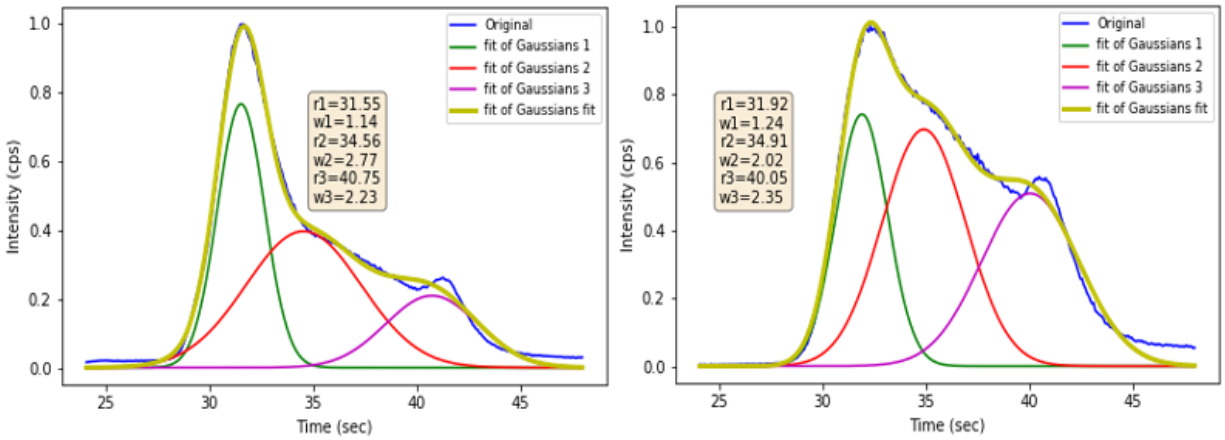

Fig. 6. Vanadium GPC-ICP HR MS normalized profiles in THF (left) and $CHCl_3$ (right) and the Gaussians fit of the HMW, MMW and LMW regions. Sulfur GPC-ICP HR MS Gaussian fit for the chromatograms obtained in THF and in $CHCl_3$ are given in in supporting information Fig. S7 and S8.

Table 2. Fitting parameters for asphaltenes in both solvents, where α is the fitting parameter, γ is the surface energy or interfacial tension calculated from Equation 3 and using ratio r

Solvent		LMW	MMW	HMW
$CHCl_3$	α	2.7	13.88	60.52
	$\gamma\ (mJ/m^2)$	0.0124	0.0168	0.044
	r (nm)	8.52	16.49	21.14
THF	α	2.31	7.85	76.09
	$\gamma\ (mJ/m^2)$	0.0130	0.0089	0.0530
	r (nm)	7.44	17.04	21.71

3.4 Adsorption Experiment in Toluene

Asphaltene adsorption experiments are focused on determining the amount of asphaltenes that are adsorbed onto nanoparticles. These experiments are usually performed to determine the efficiency of these nanoparticles to be used as adsorbents, or many reports in the literature focus on associating the efficiency with properties of the nanoparticles such as their size and composition [17,37–42]. In our experiment, we focused on studying the interaction of the nanoparticles with different aggregates that are in equilibrium in an asphaltene dispersion [16]. Fig. 7A shows the vanadium GPC-ICP HR MS profiles of Hamaca asphaltene solutions after being in contact with different percentages of silica nanoparticles. As shown in plot A, for percentages below 0.5%, a homogeneous decrease in the signal is observed; at higher percentages of nanoparticles, a significant decrease in the high-molecular-weight fraction and a relative increase in the low-molecular-weight fraction are observed. Plot 7B shows the UV–visible spectrum for each sample, where a decrease in magnitude of the spectrum is observed when the amount of adsorbent increases. Plot 7C shows the variation in the absorbance at 450 nm, which indicates a typical exponential decay for these systems. Both plots 7B and 7C show the typical adsorption behavior of asphaltenes, as presented in the literature. This result is the average behavior of the system without considering the individual behavior of different distributions that compose the sample. The curves in plot A show how the areas corresponding to the high-molecular-weight zone decrease, while the low-molecular-weight zone has a relative increase.

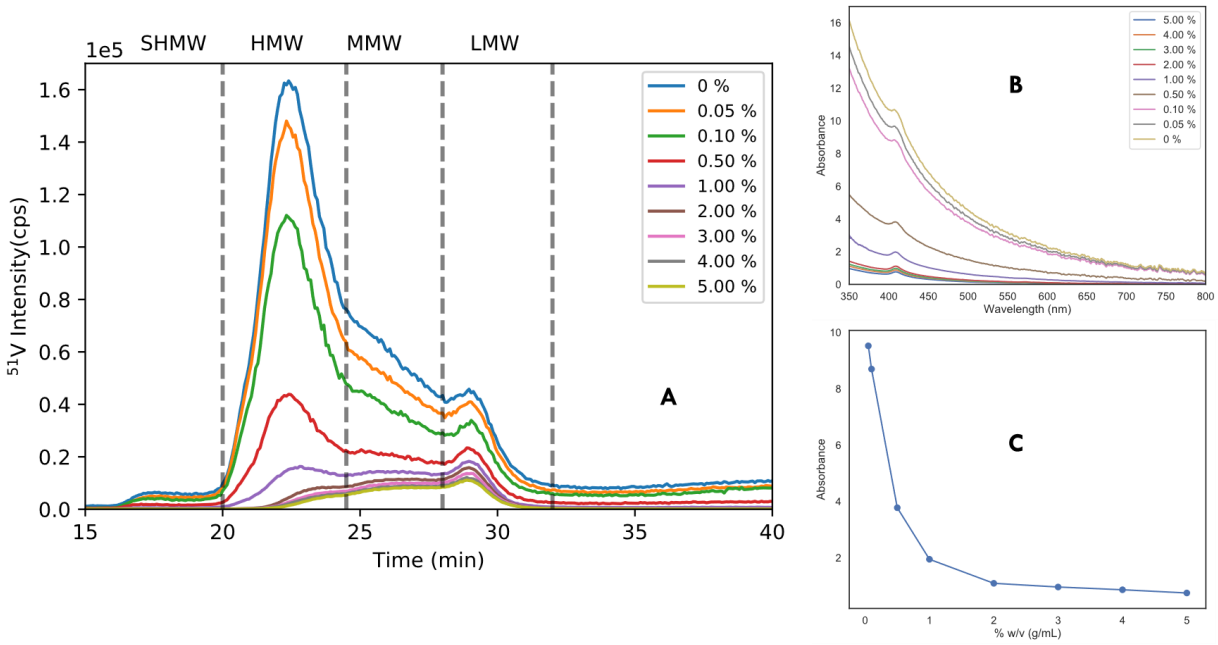

409

410 **Fig. 7**. Hamaca asphaltenes adsorption onto silica nanoparticles in toluene. Vanadium GPC-ICP
411 HR MS chromatogram (A) and UV spectrum (B) for the asphaltene and the remaining asphaltene
412 solution after contacting 0.05 to 5% NPs. Variation of the UV absorbance with w. S and Ni
413 GPC-ICP HR MS chromatogram are given in supporting information Fig. S3 for CERRO
414 NEGRO and Fig. S4 for Hamaca.

415

416 ***3.5 Adsorption Experiment in $CHCl_3$***

417 Fig. 8A shows the vanadium GPC-ICP HR MS chromatograms of Hamaca crude asphaltene
418 solutions in chloroform after being in contact with different percentages of silica
419 nanoparticles. As shown in plot 8A, for percentages below 0.5%, a homogeneous decrease
420 in the signal is observed; at higher percentages of nanoparticles, a significant decrease in the
421 high-molecular-weight fraction and a relative increase in proportion of the low-molecular-
422 weight fraction are observed. Plot B shows the UV–visible spectrum for each sample, where
423 a decrease in magnitude of the spectrum is observed when the adsorbent amount increases.

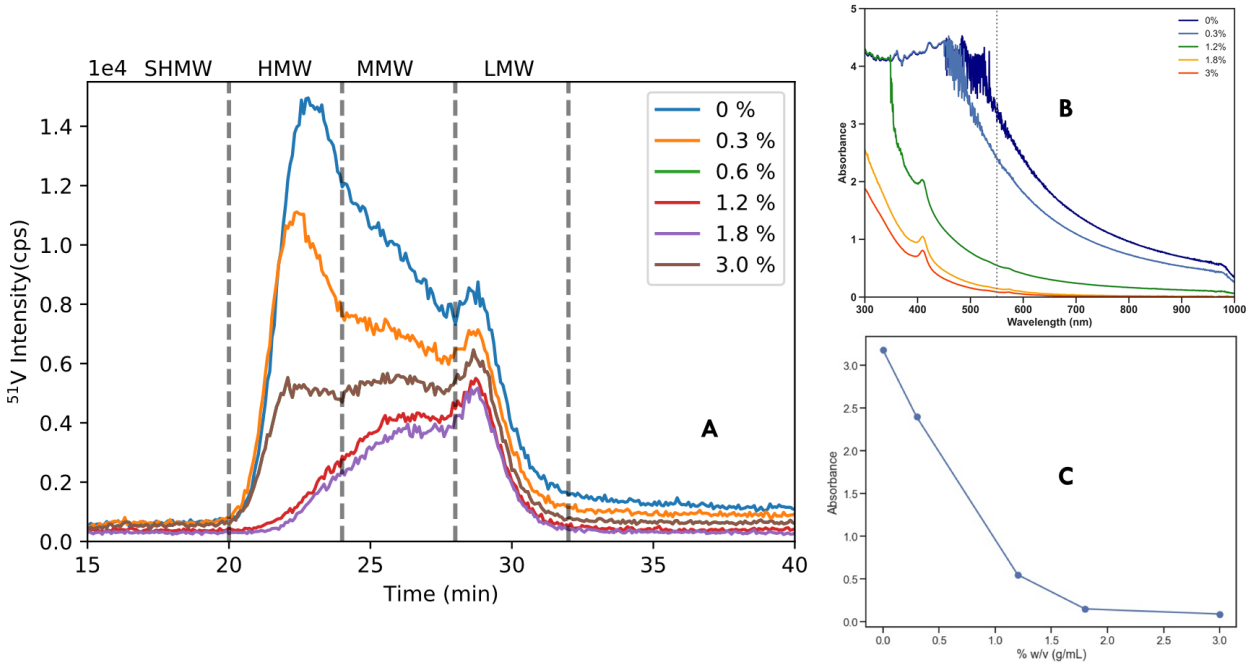

424

425 **Fig. 8**. Hamaca Asphaltene adsorption onto silica nanoparticles in chloroform. Vanadium GPC
426 ICP HR MS chromatogram (A) and UV spectrum (B) for asphaltene and the remaining
427 asphaltene solution after contacting 0.3 to 3% NPs. Variation of the UV absorbance w.

428 Fig. 9 shows the adsorption experiments of Hamaca and Cerro Negro asphaltenes and
429 their subfractions A1 and A2 in $CHCl_3$ at concentrations of 600 mg L^{-1} and 300 (mg/L)
430 nanoparticles. The first column shows the results for Hamaca, and the second column shows the
431 results for Cerro Negro. For all cases, the signals of the original solution, solution after
432 adsorption, and extracted fraction of nanoparticles after adsorption are plotted. In all cases, the
433 behavior is similar; the fraction after adsorption shows a significant decrease in intensity in the
434 section corresponding to the high-molecular-weight zone, and the fraction extracted from the
435 nanoparticles shows a higher signal in the high-molecular-weight zone. This behavior is
436 consistent with the hypotheses, where two important points have been emphasized: the fraction
437 adsorbed on the nanoparticles is the high-molecular-weight nanoaggregate or larger-

hydrodynamic-volume nanoaggregate, and the nanoaggregates remain unaltered even after adsorption.

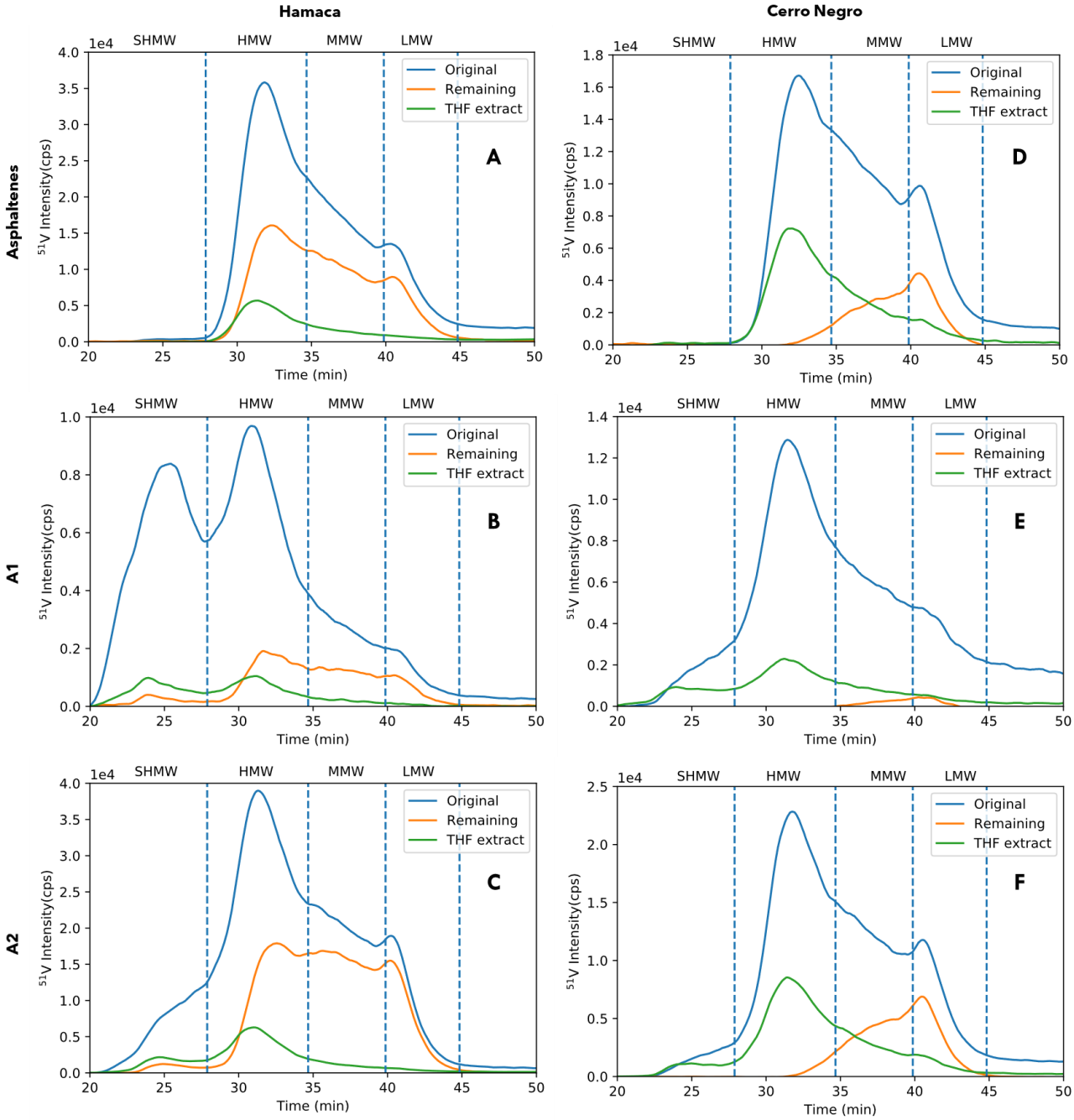

Fig. 9. Vanadium GPC-ICP HR MS chromatogram obtained during adsorption experiment in $CHCl_3$ for Hamaca asphaltene and subfractions (left) and Cerro Negro asphaltene and

subfractions (right). The S GPC-ICP MS results are given in supplemental information Fig. S9.

In Fig. 10, a scheme of the adsorption model is presented, which is very close to the observed results. Initially, different aggregates are dispersed in the solution with the highly porous nanoparticles. After adsorption, the larger components occupy the pores of the nanoparticle, and the remaining surface is left to small aggregates because the nanoparticles have a porosity of 78%, and there are very few spaces for the small and medium aggregates.

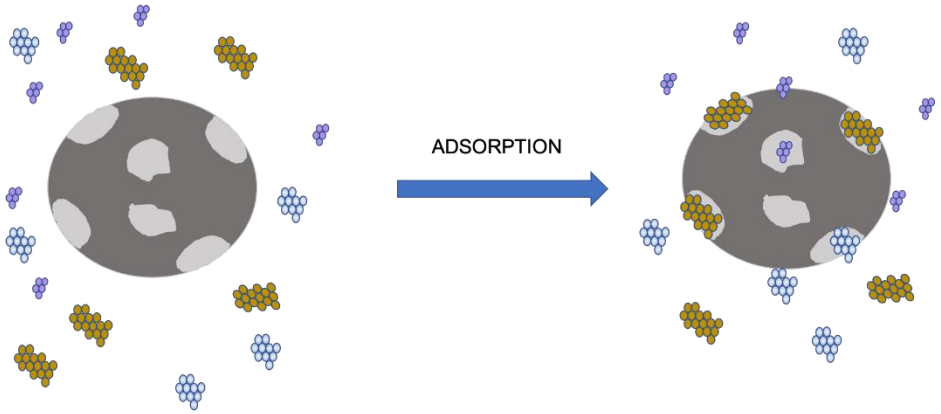

Fig. 10. Adsorption model of asphaltenes aggregates on NPs.

4 Conclusions and Final Comments

The results in this work show that asphaltenes are present in the form of aggregates of different hydrodynamic volumes in different solvents. The measurements with different solvents show that there is no critical aggregation concentration, as formally defined, since different molecular distributions proportionally dilute, which suggests that the interaction forces responsible for stabilizing them in the medium are greater than solvation and solubilization. The results show that for different solvents, there are different aggregate volume distributions. A shift to a larger hydrodynamic volume is observed when the solvency power of the solvent is lower, which indicates the increase in interaction forces between the aggregates. Our results demonstrate that

the nanoparticles preferentially adsorb the larger or heavier fractions of the asphaltenes. The adsorption process is primarily mediated by interparticle (asphaltene nanoaggregate – silica nanoparticle) interactions instead of being a typical adsorption process mediated by the active center adsorption type. The adsorption experiments in different solvents for asphaltenes and their subfractions A1 and A2 show that for polar solvents such as THF, the stabilization of the solvent on the aggregates is more important than the interaction energies, while the same experiments in toluene or $CHCl_3$ exhibit a different behavior. Toluene can dissolve them because it can enter the structure of the aggregates and enhance the stabilization.

Acknowledgements

The financial support of the Conseil Régional d'Aquitaine (20071303002PFM) and the Fonds Européen de Développement Economique et Regional (FEDER) (31486/08011464) is acknowledged.

References

[1] Boussingault J-B. Mémoire sur la composition des bitumes. Annales de Chimie Physique, 1837;64:141.

[2] Schuler B, Meyer G, Peña D, Mullins OC, Gross L. Unraveling the Molecular Structures of Asphaltenes by Atomic Force Microscopy. Journal of the American Chemical Society 2015;137:9870–6. https://doi.org/10.1021/jacs.5b04056.

[3] Putman JC, Gutiérrez Sama S, Barrère-Mangote C, Rodgers RP, Lobinski R, Marshall AG, et al. Analysis of Petroleum Products by Gel Permeation Chromatography Coupled Online with Inductively Coupled Plasma Mass Spectrometry and Offline with Fourier

Transform Ion Cyclotron Resonance Mass Spectrometry. Energy and Fuels 2018;32:12198–204. https://doi.org/10.1021/acs.energyfuels.8b02788.

[4] Gray MR, Tykwinski RR, Stryker JM, Tan X. Supramolecular assembly model for aggregation of petroleum asphaltenes. Energy and Fuels 2011;25:3125–34. https://doi.org/10.1021/ef200654p.

[5] Goncalves S, Castillo J, Fernández A, Hung J. Absorbance and fluorescence spectroscopy on the aggregation behavior of asphaltene-toluene solutions. Fuel 2004;83:1823–8. https://doi.org/10.1016/j.fuel.2004.03.009.

[6] Evdokimov IN, Fesan AA. Multi-step formation of asphaltene colloids in dilute solutions. Colloids and Surfaces A: Physicochemical and Engineering Aspects 2016;492:170–80. https://doi.org/10.1016/j.colsurfa.2015.11.072.

[7] Painter P, Veytsman B, Youtcheff J. Asphaltene aggregation and solubility. Energy and Fuels 2015;29:2120–33. https://doi.org/10.1021/ef5024912.

[8] Acevedo S, Castro A, Vásquez E, Marcano F, Ranaudo MA. Investigation of physical chemistry properties of asphaltenes using solubility parameters of asphaltenes and their fractions A1 and A2. Energy and Fuels 2010;24:5921–33. https://doi.org/10.1021/ef1005786.

[9] Castillo J, Ranaudo MAA, Fernández A, Piscitelli V, Maza M, Navarro A. Study of the aggregation and adsorption of asphaltene sub-fractions A1 and A2 by white light interferometry: Importance of A1 sub-fraction in the aggregation process. Colloids and Surfaces A: Physicochemical and Engineering Aspects 2013;427:41–6. https://doi.org/10.1016/j.colsurfa.2013.03.016.

[10] Castillo J, Fernández A, Ranaudo MA, Acevedo S. New techniques and methods for the

study of aggregation, adsorption, and solubility of asphaltenes. Impact of these properties on colloidal structure and flocculation. Petroleum Science and Technology 2001;19:75–106. https://doi.org/10.1081/LFT-100001227.

[11] Acevedo S, Guzmán K, Labrador H, Carrier H, Bouyssiere B, Lobinski R. Trapping of metallic porphyrins by asphaltene aggregates: A size exclusion microchromatography with high-resolution inductively coupled plasma mass spectrometric detection study. Energy and Fuels 2012;26:4968–77. https://doi.org/10.1021/ef3002857.

[12] Acevedo S, Castillo J, Vargas V, Castro A, Delgado O, Cortés FB, et al. Suppression of Phase Separation as a Hypothesis to Account for Nuclei or Nanoaggregate Formation by Asphaltenes in Toluene. Energy and Fuels 2018;32:6669–77. https://doi.org/10.1021/acs.energyfuels.8b00949.

[13] Nassar NN, Betancur S, Acevedo SA, Franco C, Cortés FB. Development of a Population Balance Model to Describe the Influence of Shear and Nanoparticles on the Aggregation and Fragmentation of Asphaltene Aggregates. Industrial & Engineering Chemistry Research 2015:150808100708002. https://doi.org/10.1021/acs.iecr.5b02075.

[14] Hosseinpour N, Khodadadi AA, Bahramian A, Mortazavi Y. Asphaltene adsorption onto acidic/basic metal oxide nanoparticles toward in situ upgrading of reservoir oils by nanotechnology. Langmuir 2013;29:14135–46. https://doi.org/10.1021/la402979h.

[15] Montoya T, Argel BL, Nassar NN, Franco CA, Cort??s FB. Kinetics and mechanisms of the catalytic thermal cracking of asphaltenes adsorbed on supported nanoparticles. Petroleum Science 2016;13:561–71. https://doi.org/10.1007/s12182-016-0100-y.

[16] Castillo J, Vargas V, Gonzalez G, Ruiz W, Bouyssiere B. Evidence of selective asphaltene subfraction adsorption on SiO2 nanoparticles studied by UV-vis absorbance and

fluorescence spectroscopy. Journal of Dispersion Science and Technology 2020:1–7. https://doi.org/10.1080/01932691.2020.1845956.

[17] Mirzayi B, Shayan NN. Adsorption kinetics and catalytic oxidation of asphaltene on synthesized maghemite nanoparticles. Journal of Petroleum Science and Engineering 2014. https://doi.org/10.1016/j.petrol.2014.06.031.

[18] Castillo J, Vargas V, Gonzalez G, Ruiz W, Gascon G, Bouyssiere B. Development of a Methodology Using GPC-ICP HR MS for Analysis of the Adsorption of Asphaltene Aggregates on SiO 2 Nanoparticles. Energy & Fuels 2020;34:6920–7. https://doi.org/10.1021/acs.energyfuels.0c00714.

[19] Nassar NN. Asphaltene Adsorption onto Alumina Nanoparticles: Kinetics and Thermodynamic Studies. Energy & Fuels 2010;24:4116–22. https://doi.org/10.1021/ef100458g.

[20] Guzmán JD, Betancur S, Carrasco-Marín F, Franco CA, Nassar NN, Cortés FB. Importance of the Adsorption Method Used for Obtaining the Nanoparticle Dosage for Asphaltene-Related Treatments. Energy and Fuels 2016;30:2052–9. https://doi.org/10.1021/acs.energyfuels.5b02841.

[21] Franco CA, Lozano MM, Acevedo S, Nassar NN, Cortés FB. Effects of Resin i on Asphaltene Adsorption onto Nanoparticles: A Novel Method for Obtaining Asphaltenes/Resin Isotherms. Energy and Fuels 2016;30:264–72. https://doi.org/10.1021/acs.energyfuels.5b02504.

[22] Cheng B, Zhao J, Yang C, Tian Y, Liao Z. Geochemical Evolution of Occluded Hydrocarbons inside Geomacromolecules: A Review. Energy and Fuels 2017;31:8823–32. https://doi.org/10.1021/acs.energyfuels.7b00454.

[23] Moncayo-Riascos I, Lozano MM, Hoyos BA, Franco CA, Riazi M, Cortés FB. Physical Insights about Viscosity Differences of Asphaltene Dissolved in Benzene and Xylene Isomers: Theoretical-Experimental Approaches. Energy and Fuels 2021;35:18574–82. https://doi.org/10.1021/acs.energyfuels.1c03348.

[24] Jiang B, Zhang R, Yang N, Zhang L, Sun Y. Asphaltene Aggregation and Assembly Behaviors in Organic Solvents with Water and Inhibitor. Energy and Fuels 2019;33:1955–68. https://doi.org/10.1021/ACS.ENERGYFUELS.8B04121/SUPPL_FILE/EF8B04121_SI_001.PDF.

[25] Xiong Y, Cao T, Chen Q, Li Z, Yang Y, Xu S, et al. Adsorption of a Polyaromatic Compound on Silica Surfaces from Organic Solvents Studied by Molecular Dynamics Simulation and AFM Imaging. Journal of Physical Chemistry C 2017;121:5020–8. https://doi.org/10.1021/ACS.JPCC.6B11763/SUPPL_FILE/JP6B11763_SI_001.PDF.

[26] Gutiérrez LB, Ranaudo MA, Méndez B, Acevedo S. Fractionation of asphaltene by complex formation with p-nitrophenol. A method for structural studies and stability of asphaltene colloids. Energy and Fuels 2001;15:624–8. https://doi.org/10.1021/ef000180y.

[27] Acevedo N, Vargas V, Piscitelli V, Bouyssiere B, Carrier H, Castillo J. SiO 2 Biogenic Nanoparticles and Asphaltenes: Interactions and Their Consequences Investigated by QCR and GPC-ICP-HR-MS. Energy & Fuels 2021;35:6566–75. https://doi.org/10.1021/acs.energyfuels.0c04185.

[28] González G, Acevedo S, Castillo J, Villegas O, Ranaudo MA, Guzmán K, et al. Study of Very High Molecular Weight Cluster Presence in THF Solution of Asphaltenes and Subfractions A1 and A2, by Gel Permeation Chromatography with Inductively Coupled

Plasma Mass Spectrometry. Energy and Fuels 2020;34:12535–44. https://doi.org/10.1021/acs.energyfuels.0c02743.

[29] Yarranton HW, Ortiz DP, Barrera DM, Baydak EN, Barré L, Frot D, et al. On the size distribution of self-associated asphaltenes. Energy and Fuels 2013;27:5083–106. https://doi.org/10.1021/ef400729w.

[30] Murray Gray and Harvey W. Yarranton. Quantitative Modelling of Formation of Asphaltene Nanoaggregates. Energy and Fuels 2019;33:8566-8575.https://doi.org: 10.1021/acs.energyfuels.9b02400

[31] Chaisoontornyotin W, Haji-Akbari N, Fogler HS, Hoepfner MP. Combined Asphaltene Aggregation and Deposition Investigation. Energy and Fuels 2016;30:1979–86. https://doi.org/10.1021/acs.energyfuels.5b02427.

[32] Hoepfner MP, Vilas Boîas Fávero C, Haji-Akbari N, Fogler HS. The fractal aggregation of asphaltenes. Langmuir 2013;29:8799–808. https://doi.org/10.1021/la401406k.

[33] Gascon G, Vargas V, Feo L, Castellano O, Castillo J, Giusti P, et al. Size Distributions of Sulfur, Vanadium, and Nickel Compounds in Crude Oils, Residues, and Their Saturate, Aromatic, Resin, and Asphaltene Fractions Determined by Gel Permeation Chromatography Inductively Coupled Plasma High-Resolution Mass Spectrometry. Energy and Fuels 2017;31:7783–8. https://doi.org/10.1021/acs.energyfuels.7b00527.

[34] Putman JC, Moulian R, Barrère-Mangote C, Rodgers RP, BOUYSSIERE B, Giusti P, et al. Probing Aggregation Tendencies in Asphaltenes by Gel Permeation Chromatography. Part 1: Online Inductively Coupled Plasma Mass Spectrometry and Offline Fourier Transform Ion Cyclotron Resonance Mass Spectrometry. Energy & Fuels 2020. https://doi.org/10.1021/acs.energyfuels.0c01522.

[35] Caumette G, Lienemann C, Merdrignac I, Bouyssiere B, Lobinski R. Fractionation and speciation of nickel and vanadium in crude oils by size exclusion chromatography-ICP MS and normal phase HPLC-ICP MS. Journal of Analytical Atomic Spectrometry 2010;25:1123–9. https://doi.org/10.1039/c003455j.

[36] Castillo J, Vargas V. Metal porphyrin occlusion: Adsorption during asphaltene aggregation. Petroleum Science and Technology 2016;34. https://doi.org/10.1080/10916466.2016.1170846.

[37] Abu Tarboush BJ, Husein MM. Adsorption of asphaltenes from heavy oil onto in situ prepared NiO nanoparticles. Journal of colloid and interface science 2012;378:64–9. https://doi.org/10.1016/j.jcis.2012.04.016.

[38] Vargas V, Castillo J, Ocampo-Torres R, Lienemann CP, Bouyssiere B. Surface modification of SiO2 nanoparticles to increase asphaltene adsorption. Petroleum Science and Technology 2018;36:618–24. https://doi.org/10.1080/10916466.2018.1440300.

[39] Montes D, Henao J, Taborda EA, Gallego J, Cortés FB, Franco CA. Effect of Textural Properties and Surface Chemical Nature of Silica Nanoparticles from Different Silicon Sources on the Viscosity Reduction of Heavy Crude Oil. ACS Omega 2020;5:5085–97. https://doi.org/10.1021/acsomega.9b04041.

[40] Montoya T, Coral D, Franco C a, Nassar NN, Cortés FB. A Novel Solid–Liquid Equilibrium Model for Describing the Adsorption of Associating Asphaltene Molecules onto Solid Surfaces Based on the “Chemical Theory”. Energy & Fuels 2014;28:4963–75. https://doi.org/10.1021/ef501020d.

[41] Mejia JM, Ruiz MA, Benjumea P, Riffel DB, Cortes FB. Sorption of Asphaltenes onto Nanoparticles of Nickel Oxide Supported on Nanoparticulated Silica Gel. Energy and

Fuels 2012;26:1725–30.

[42] Sepideh Kashefi, Lotfollahi MN, Shahrabadi A. Asphaltene Adsorption using Nanoparticles with Different Surface Chemistry: Equilibrium and Thermodynamics Studies. Petroleum Chemistry 2019;59:1201–6. https://doi.org/10.1134/S0965544119110124.

[43] Jamshidian M, Thamburaja P, Rabczuk T. A continuum state variable theory to model the size-dependent surface energy of nanostructures. Phys Chem Chem Phys 2015;17:25494–8. https://doi.org/10.1039/C5CP04375A.

[44] Jia L, Shi B. A New Equation between Surface Tensions and Solubility Parameters without Molar Volume Parameters Simultaneously Fitting Polymers and Solvents. Journal of Macromolecular Science, Part B 2011;50:1042–6. https://doi.org/10.1080/00222348.2010.497439.

[45] Xiong Y, Cao T, Chen Q, Li Z, Yang Y, Xu S, et al. Adsorption of a Polyaromatic Compound on Silica Surfaces from Organic Solvents Studied by Molecular Dynamics Simulation and AFM Imaging. J Phys Chem C 2017;121:5020–8. https://doi.org/10.1021/acs.jpcc.6b11763.

[46] Jiang B, Zhang R, Yang N, Zhang L, Sun Y. Asphaltene Aggregation and Assembly Behaviors in Organic Solvents with Water and Inhibitor. Energy Fuels 2019;33:1955–68. https://doi.org/10.1021/acs.energyfuels.8b04121.

[47] Yu W, Hou W. Correlations of surface free energy and solubility parameters for solid substances. Journal of Colloid and Interface Science 2019;544:8–13. https://doi.org/10.1016/j.jcis.2019.02.074.

[48] Nategh M, Mahdiyar H, Malayeri MR, Binazadeh M. Impact of Asphaltene Surface

Energy on Stability of Asphaltene–Toluene System: A Parametric Study. Langmuir 2018;34:13845–54. https://doi.org/10.1021/acs.langmuir.8b02566.

[49] Samsonov V, Bazulev A, Sdobnyakov N. On applicability of Gibbs thermodynamics to nanoparticles. Open Physics 2003;1:474–84. https://doi.org/10.2478/BF02475858.

[50] Samsonov VM, Chernyshova AA, Sdobnyakov NYu. Size dependence of the surface energy and surface tension of metal nanoparticles. Bull Russ Acad Sci Phys 2016;80:698–701. https://doi.org/10.3103/S1062873816060290.

[51] Vollath D, Fischer FD, Holec D. Surface energy of nanoparticles – influence of particle size and structure. Beilstein J Nanotechnol 2018;9:2265–76. https://doi.org/10.3762/bjnano.9.211.